

# Surface Topography: Metrology and Properties



## PAPER

### Laser recovery of grinding-induced subsurface damage in the edge and notch of a single-crystal silicon wafer

RECEIVED  
3 November 2018

REVISED  
17 December 2018

ACCEPTED FOR PUBLICATION  
14 January 2019

PUBLISHED  
7 February 2019

Keiichiro Niitsu<sup>1</sup>, Yu Tayama<sup>2</sup>, Takatoshi Kato<sup>2</sup> and Jiwang Yan<sup>3</sup>

<sup>1</sup> School of Integrated Design Engineering, Graduate School of Science and Technology, Keio University, Hiyoshi 3-14-1, Kohoku-ku, Yokohama 223-8522, Japan

<sup>2</sup> SPEEDFAM Co., Ltd, Ohgami 4-2-37, Ayase 252-1104, Kanagawa, Japan

<sup>3</sup> Department of Mechanical Engineering, Faculty of Science and Technology, Keio University, Hiyoshi 3-14-1, Kohoku-ku, Yokohama 223-8522, Japan

E-mail: [yan@mech.keio.ac.jp](mailto:yan@mech.keio.ac.jp)

**Keywords:** single-crystal silicon, laser recovery, wafer edge, subsurface damage, surface topography, curved surface

## Abstract

The edges and notches of silicon wafers are usually machined by diamond grinding, and the grinding-induced subsurface damage causes wafer breakage and particle contamination problems. However, the edge and notch surfaces have large curvature and sharp corners, thus it is difficult to be finished by chemo-mechanical polishing. In this study, a nanosecond pulsed Nd:YAG laser was used to irradiate the edge and notch of a boron-doped single-crystal silicon wafer to recover the grinding-induced subsurface damage. The reflection loss and the change of laser fluence when irradiating a curved surface were considered, and the damage recovery behavior was investigated. The surface roughness, crystallinity, and hardness of the laser recovered region were measured by using white light interferometry, laser micro-Raman spectroscopy, and nanoindentation, respectively. The results showed that after laser irradiation the damaged region was recovered to a single-crystal structure with nanometric surface roughness, and the surface hardness was also improved. This study demonstrates that laser recovery is a promising post-grinding process for improving the surface integrity of the edge and notch of silicon wafers.

## 1. Introduction

Single-crystal silicon is a useful and essential material in the semiconductor industry. Generally, silicon wafers are produced by ingot slicing, edge/notch grinding, surface grinding, edge/notch polishing, and surface polishing processes etc. Slicing and grinding processes induce subsurface damages, such as phase transformations, dislocations, and microcracks, in silicon wafers [1–3]. Subsurface damages in plane wafer surfaces can be removed by polishing, while wafer edges and notches are very difficult to polish due to their special shapes. For example, full round edges have been used for preventing breakage to replace sharp edges [4–6]. However, required by chemo-mechanical polishing (CMP) for inter-level dielectric planarization, blunter edge shapes were employed [7]. A wafer edge with a trapezoidal surface and a circular top, as shown in figure 1(a), is now popular. Meanwhile, a wafer notch having a chamfered V-shape, which is similar to hyperbolic paraboloid as shown in

figure 1(b), is required. These edge and notch shapes are very difficult to grind even if the same abrasive grain size as that in grinding plane surfaces is used because the shape of grinding wheels and grinding conditions are distinctly different for these surfaces. Thus, the resulting edge and notch surfaces have more severe subsurface damages than plane surfaces.

Though the edge and notch regions of a silicon wafer are not used directly for electronic device fabrication, grinding-induced subsurface damages in these regions may cause wafer breakage and particle contamination problems. In order to completely eliminate the subsurface damages, CMP has been necessary. However, the material removal depth for the edge and notch in CMP is larger than that for the plane surface. This makes the CMP of wafer edges and notches extremely expensive, which is a big problem in silicon wafer manufacturing [8].

In our previous research, laser recovery was proposed to eliminate the subsurface damages generated by diamond cutting and grinding in single-crystal

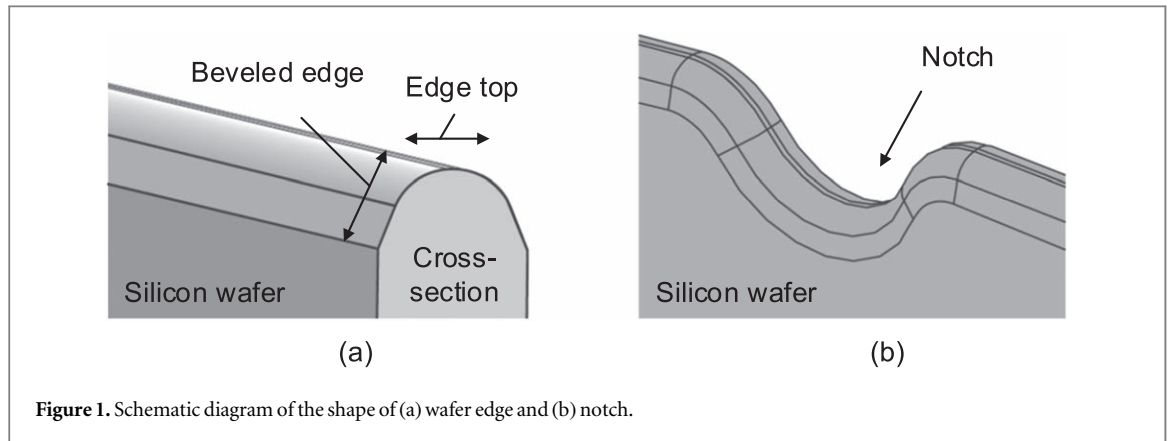


Figure 1. Schematic diagram of the shape of (a) wafer edge and (b) notch.

wafers [9–12]. Laser recovery technology involves selectively melting and recrystallizing of the machining-damaged subsurface layers including amorphous layers, dislocations, and microcracks. After laser irradiation, a single-crystalline structure is reproduced by epitaxial growth from the undamaged bulk. In addition, laser recovery technology can create a smoother surface in comparison with a grinding finish. Thus, laser recovery technology is anticipated to be also applicable to improving the surface integrity of wafer edges and notches having complicated shapes. However, up to date, laser irradiation has been performed perpendicularly to a silicon surface even the surface is curved [11], where special systems for controlling laser incident angle and wafer position is needed. Thus, wafer manufacturing equipment is complicated and difficult to be realized for recovering complicated shapes or sharply cornered structures like wafer notches.

The purpose of this study is to explore the possibility of recovering grinding-induced subsurface damage in wafer edges and notches without making the laser beam perpendicular to the surface. Laser irradiation experiment was attempted at different angles of incident to a curved or angled surface, and laser recovery characteristics were investigated by considering the reflectivity and laser fluence change under various conditions. Furthermore, the laser recovery mechanism of grinding-induced microcracks, which is a typical subsurface damage for wafer notches, was experimentally clarified. The success of the proposed method will contribute to reducing the manufacturing cost and improving the surface integrity of silicon wafers.

## 2. Process modeling

### 2.1. Mechanism of laser recovery

Figure 2 shows the laser recovery mechanism of subsurface damages in ground silicon [12]. In general, grinding process induces subsurface damages such as amorphous layers, dislocations, and microcracks (figure 2(a)). During laser irradiation, a top-down

melted layer is generated (figure 2(b)). The melting layer becomes increasingly thicker and finally reaches the defect-free bulk region (figure 2(c)). It is worth mentioning the depth of the melting region depends on laser energy density, wavelength of the laser, pulse duration, and beam profiles, etc [12]. After laser irradiation, bottom-up epitaxial growth of silicon starts from the liquid/solid boundary (figures 2(d)–(e)). By using this method, a defect-free single-crystal structure is produced in the laser-affected region (figure 2(f)).

### 2.2. Reflectivity on beveled edge surface

When the laser is irradiated at different angles of incident to a sample surface, the reflectivity is changed, and then the change of the reflectivity affects the energy absorbed by the sample. The reflection of the laser is affected by two polarizations; p-polarization and s-polarization. If the laser irradiated perpendicular to the surface, these two polarizations cannot be distinguished. P-polarization is the plane of polarization perpendicular to the cross-section, while s-polarization is parallel to the cross-section as shown in figure 3. The reflectivity of these two polarizations are given by [13]:

$$R_p = \frac{[n - (1/\cos \theta)]^2 + \kappa}{[n + (1/\cos \theta)]^2 + \kappa} \quad (1)$$

$$R_s = \frac{[n - \cos \theta]^2 + \kappa}{[n + \cos \theta]^2 + \kappa} \quad (2)$$

where  $R_p$  is the reflectivity of p-polarization,  $R_s$  the reflectivity of s-polarization,  $n$  the refractive index, the  $\kappa$  the extinction coefficient, and  $\theta$  the angle. In the work of Zhang *et al* [14],  $n$  and  $\kappa$  at wavelength 532 nm for single-crystal silicon were calculated by interpolation as  $n = 4.12$  and  $\kappa = 2.66 \times 10^{-2}$ . Figure 4 shows the calculated reflectivity of single-crystal silicon at wavelength 532 nm. In the figure,  $R$  is mean of  $R_p$  and  $R_s$ . The beveled angle of the wafer edge  $\phi$  was  $22.5^\circ$ . Thus, laser incident angle  $\theta$  was  $67.5^\circ$ . According to equations (1) and (2), when the laser was irradiated perpendicularly to the top surface,  $R = 0.371$ . When the laser was irradiated to the beveled surface of the edge,  $R_p = 0.05$  and  $R_s = 0.689$ , hence  $R = 0.370$ . According to this calculation, the

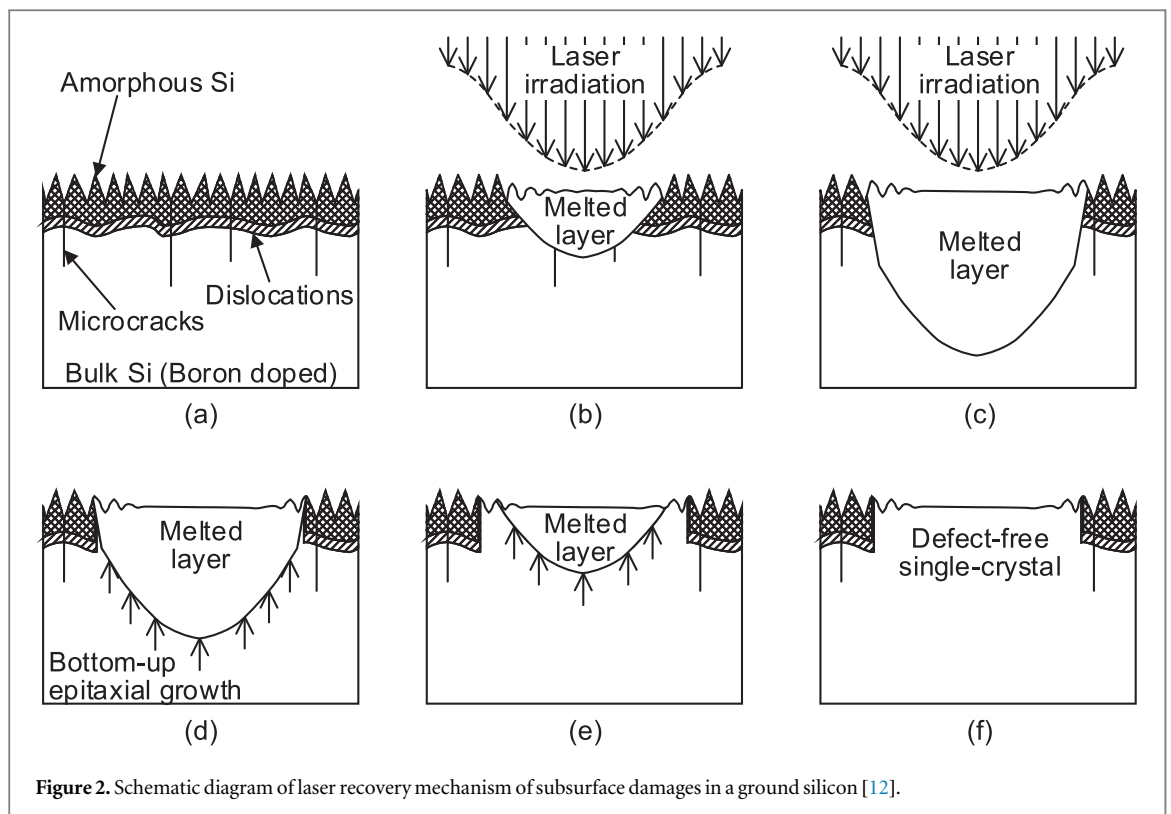


Figure 2. Schematic diagram of laser recovery mechanism of subsurface damages in a ground silicon [12].

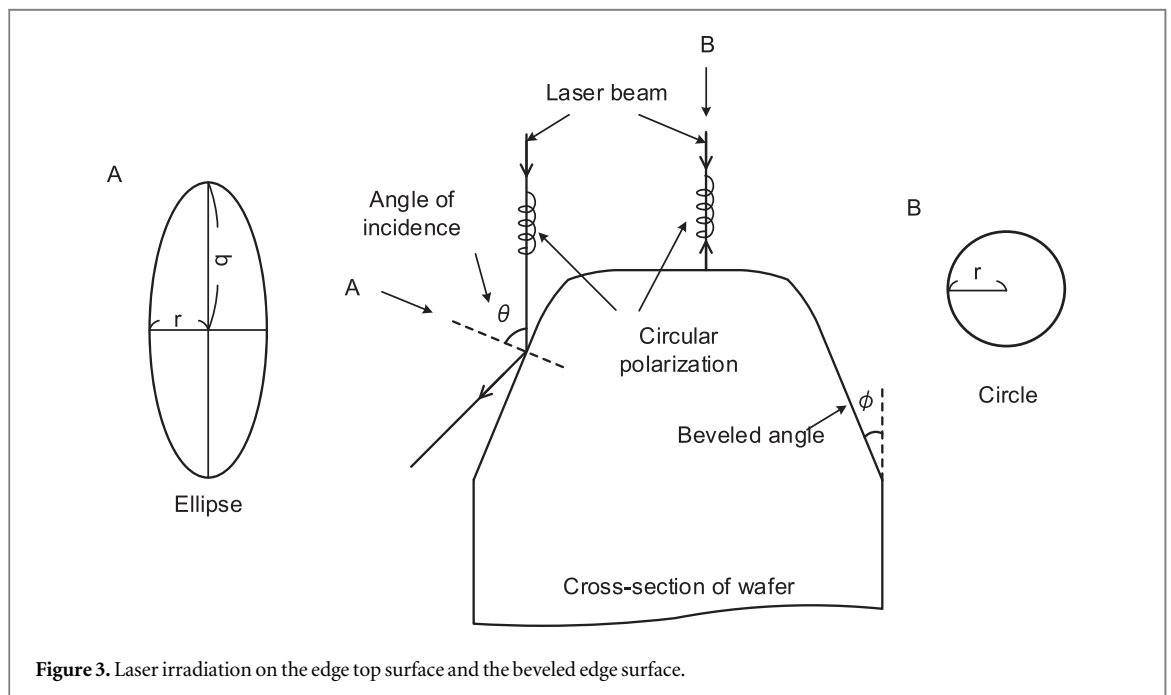


Figure 3. Laser irradiation on the edge top surface and the beveled edge surface.

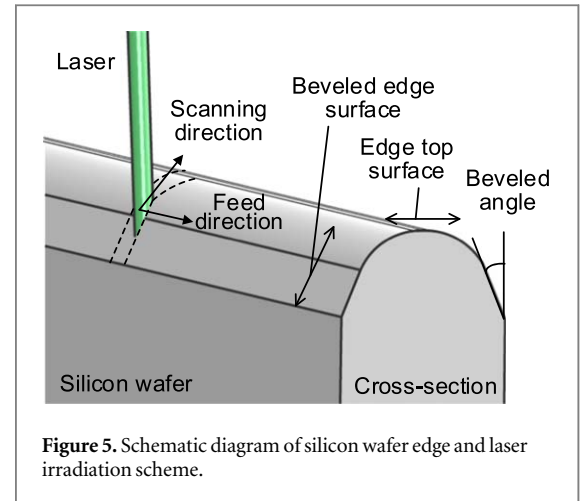
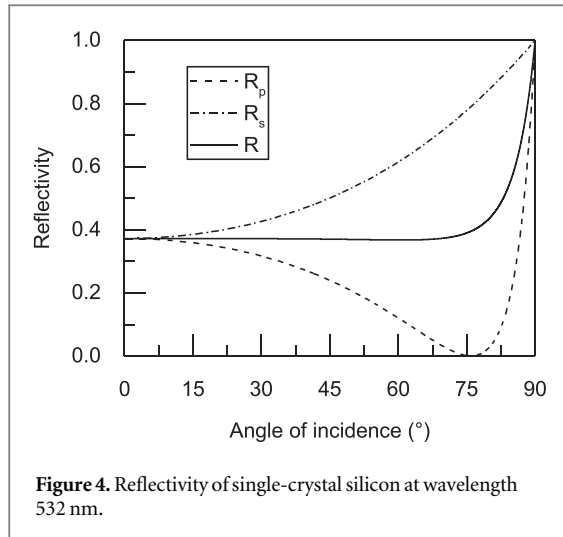
reflectivity of the beveled surface was only decreased by 0.27% in comparison with that of the top surface. Thus, the effect of reflection is insignificant in laser irradiation for the beveled edge surface.

Next, decreasing laser fluence due to changing spot area was investigated. The beam shape is a circle when irradiated on the edge top wafer, and becomes an ellipse when irradiated on the beveled edge of the wafer. Thus, it is necessary to adjust laser fluence for the beveled edge to be the same as that for the edge top.

In order to correct the laser fluence, the area ratio  $S$  is defined by:

$$S = \frac{A_e}{A_c} \tag{3}$$

where  $A_e$  is the area of the elliptic beam on the beveled edge, and  $A_c$  is the area of the circular beam on the edge top. If we suppose that the beam radius of the circle is  $r$ , and when changing an ellipse of the beam length of the semi-major axis and the semi-minor axis are  $b$  and

**Table 1.** Laser irradiation conditions for edge top surface.

Beam radius ( $\mu\text{m}$ )	42.5
Number of pulses per unit area	50
Pulse width (ns)	48.4
Repetition frequency (kHz)	10
Average power (mW)	900, 1100, 1300, 1500
Laser fluence ( $\text{J cm}^{-2}$ )	1.59, 1.94, 2.29, 2.64
Scanning speed ( $\text{mm s}^{-1}$ )	17.0
Scanning pitch ( $\mu\text{m}$ )	13.3

**Table 2.** Laser irradiation conditions for beveled edge surface.

Beam length of the semi-major axis ( $\mu\text{m}$ )	111
Beam length of the semi-minor axis ( $\mu\text{m}$ )	42.5
Repetition frequency (kHz)	10
Pulse width (ns)	48.4
Average power (mW)	900, 2350
Laser fluence ( $\text{J cm}^{-2}$ )	0.61, 1.58
Scanning speed ( $\text{mm s}^{-1}$ )	17.0
Scanning pitch ( $\mu\text{m}$ )	13.3

$r$ , respectively, then the semi-minor axis  $b$  with respect to the beveled angle of the wafer edge  $\phi$  is calculated by

$$b = \frac{r}{\sin(\phi)} \quad (4)$$

Therefore the area ratio  $S$  in equation (3) can be obtained by

$$S = \frac{\pi r b}{\pi r^2} = \frac{\pi r \frac{r}{\sin(\phi)}}{\pi r^2} = \frac{1}{\sin(\phi)} \quad (5)$$

For instance, when  $\phi = 22.5^\circ$  is substituted in equation (5),  $S = 2.61$ . When the average laser power is 900 mW, the equivalent laser fluence is  $1.59 \text{ J cm}^{-2}$  on the edge top surface whereas the equivalent laser fluence is  $0.61 \text{ J cm}^{-2}$  on the beveled edge surface because of the change of the beam shape. In order to compensate laser fluence, the average laser power

**Table 3.** Laser irradiation conditions for notch.

Beam radius ( $\mu\text{m}$ )	42.5
Repetition frequency (kHz)	10
Pulse width (ns)	48.4
Average power (mW)	900, 1200, 1500
Laser fluence ( $\text{J cm}^{-2}$ )	1.59, 2.11, 2.64
Scanning speed ( $\text{mm s}^{-1}$ )	17.0
Scanning pitch ( $\mu\text{m}$ )	13.3

**Table 4.** Laser irradiation conditions for a plane silicon wafer.

Beam radius ( $\mu\text{m}$ )	42.5
Repetition frequency (kHz)	10
Pulse width (ns)	48.4
Average power (mW)	900
Laser fluence ( $\text{J cm}^{-2}$ )	1.59
Scanning speed ( $\text{mm s}^{-1}$ )	17.0
Scanning pitch ( $\mu\text{m}$ )	13.3

must be increased to 2.61 times. This method can be used to scan the entire peripheral edge of the standard circular-shape Si wafers by slightly adjusting the angle between the laser beam and the wafer surface using a swinging mechanism.

### 3. Experimental procedures

Boron-doped P++ single-crystal silicon wafers were used as samples. The resistivity of the wafers was  $0.004 - 0.007 \Omega \cdot \text{cm}$ . The wafers were machined by precision grinding with diamond abrasive grains (average grain size  $8.5 \mu\text{m}$ ).

A Nd:YAG laser system, LR-SHG (MEGAOPTO Co., Ltd, Japan) was used for laser irradiation. The laser system was completely air cooled and a laser diode was used as the excitation light source. The wavelength is 532 nm. Laser irradiation was

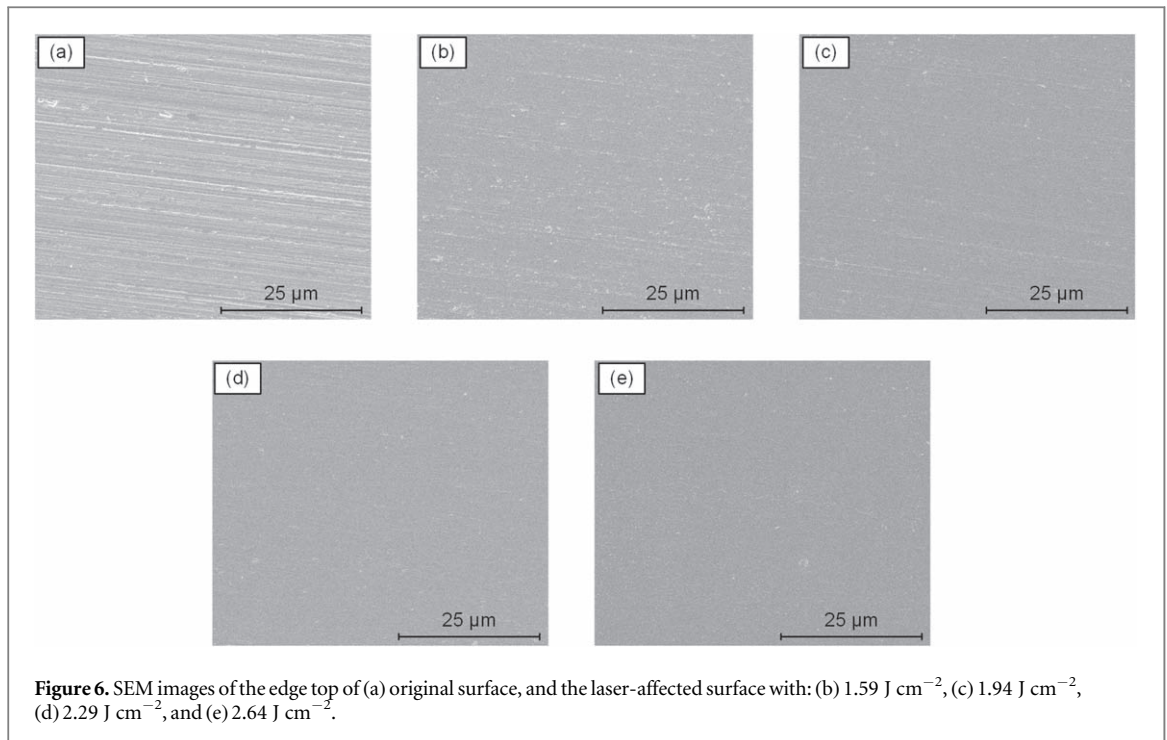


**Figure 6.** SEM images of the edge top of (a) original surface, and the laser-affected surface with: (b)  $1.59 \text{ J cm}^{-2}$ , (c)  $1.94 \text{ J cm}^{-2}$ , (d)  $2.29 \text{ J cm}^{-2}$ , and (e)  $2.64 \text{ J cm}^{-2}$ .

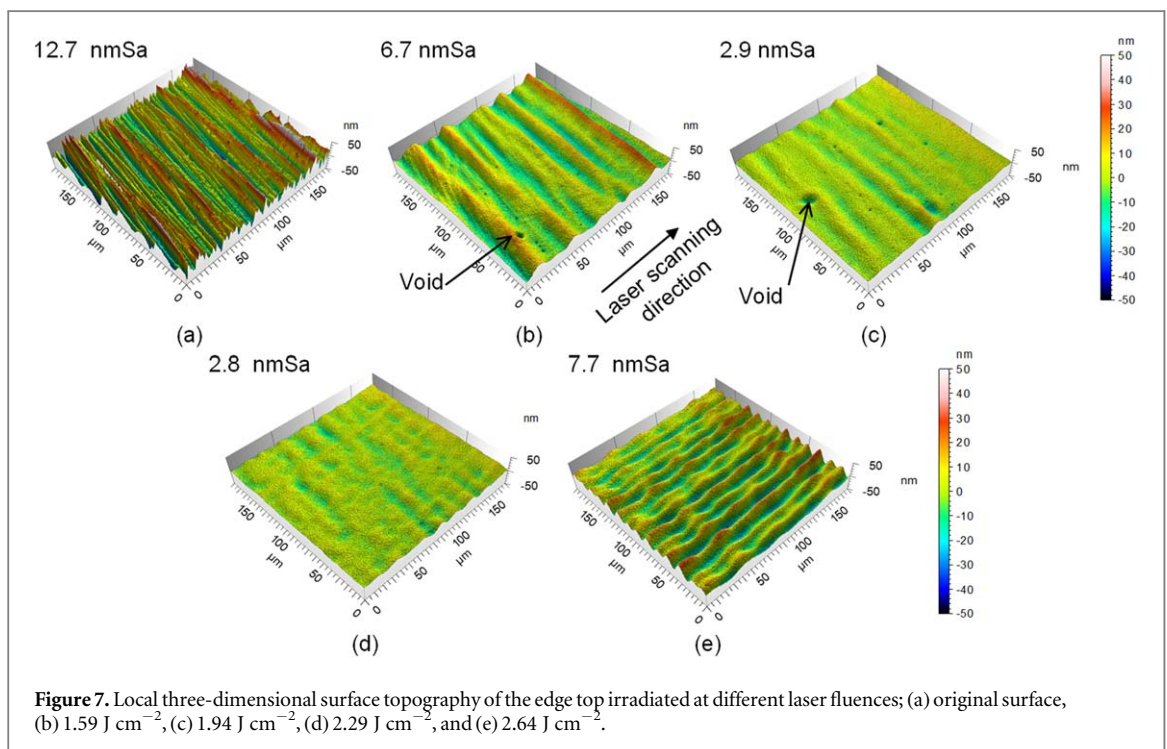


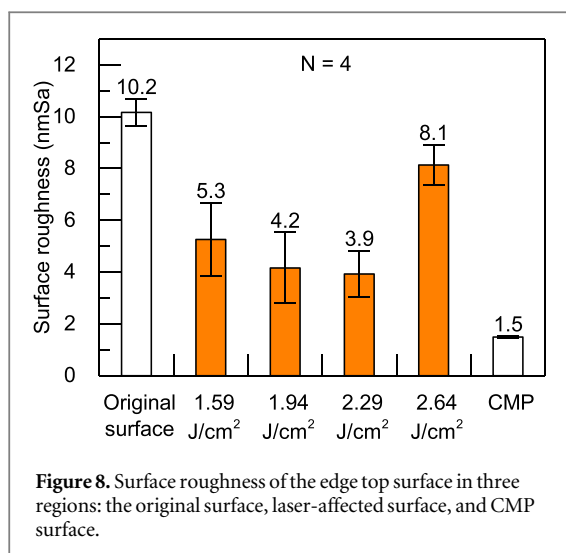
**Figure 7.** Local three-dimensional surface topography of the edge top irradiated at different laser fluences; (a) original surface, (b)  $1.59 \text{ J cm}^{-2}$ , (c)  $1.94 \text{ J cm}^{-2}$ , (d)  $2.29 \text{ J cm}^{-2}$ , and (e)  $2.64 \text{ J cm}^{-2}$ .

performed in air by computer control of the laser system and a galvanometer mirror. The laser beam has a diameter of  $85 \mu\text{m}$  and the Gaussian energy distribution.

A pulse width of  $48.4 \text{ ns}$  and a repetition frequency of  $10 \text{ kHz}$  were chosen for laser irradiation. The laser scanning speed was  $17.0 \text{ mm s}^{-1}$  and the scan pitch was  $13.3 \mu\text{m}$ . Laser irradiation path of the edge surface is shown in figure 5. Laser was irradiated at different angles of incident to both the beveled edge and the edge top surface. The laser irradiation conditions are

summarized in tables 1 and 2. Then, a wafer notch was irradiated with various average laser powers, the laser irradiation conditions for which are summarized in table 3.

After laser irradiation, the surface was observed by using a scanning electron microscope (SEM) Inspect S50 (FEI Company). The surface roughness of samples was measured by using a white-light interferometer Talysurf CCI 1000 (AMETEK Taylor Hobson Ltd, UK). The vertical resolution of the white-light interferometer was  $0.01 \text{ nm}$ , and the lateral resolution was



350 nm. In addition, a laser probe profilometer MP-3 (Mitaka Kohki Co., Ltd, Japan) was used to measure profile of notch wafer. A laser micro-Raman spectrometer NRS-3100 (JASCO Co., Japan) was used for analyzing crystallinity of the surfaces. The laser wavelength of the Raman spectrometer is 532 nm and the beam diameter is 1  $\mu\text{m}$ .

Finally, in order to evaluate the effect of laser recovery on material hardness change, the laser was irradiated perpendicularly to a plane silicon wafer. The laser irradiation conditions for a plane silicon wafer are shown in table 4. After laser irradiation, nanoindentation tests were performed for the irradiated plane wafer by using a nanoindentation instrument ENT-100a (Elionix Inc., Japan). A Berkovich-type diamond indenter was used. Indentation load was set to 3, 5, 8, 10, 15, 20, and 30 mN with a loading rate of 0.5 mN s<sup>-1</sup>. The hardness of a CMP wafer was also measured for comparison.

## 4. Results and discussion

### 4.1. Surface topography of wafer edge top

Figure 6 shows SEM images of the edge top surface before laser irradiation (figure 6(a)) and after laser irradiation with different laser fluences (figures 6(b)–(e)). The number of grinding marks decreases by laser irradiation, however, there are ridges which are partially smoothed grinding marks (figure 6(b)). When the laser fluence increased over 2.29 J cm<sup>-2</sup>, the grinding marks were completely smoothed as shown in figures 6(c) and (d). In order to evaluate surface topography for more detail, three-dimensional surface topography was measured by white light interferometry.

Figure 7 is the local three-dimensional surface topography of the edge top after filtering by a cut-off of  $\lambda = 25 \mu\text{m}$ . The surface topography of the original surface is shown in figure 7(a). As shown in figure 7(b), fine grinding marks were smoothed by laser irradiation at a laser fluence of 1.59 J cm<sup>-2</sup>, but surface

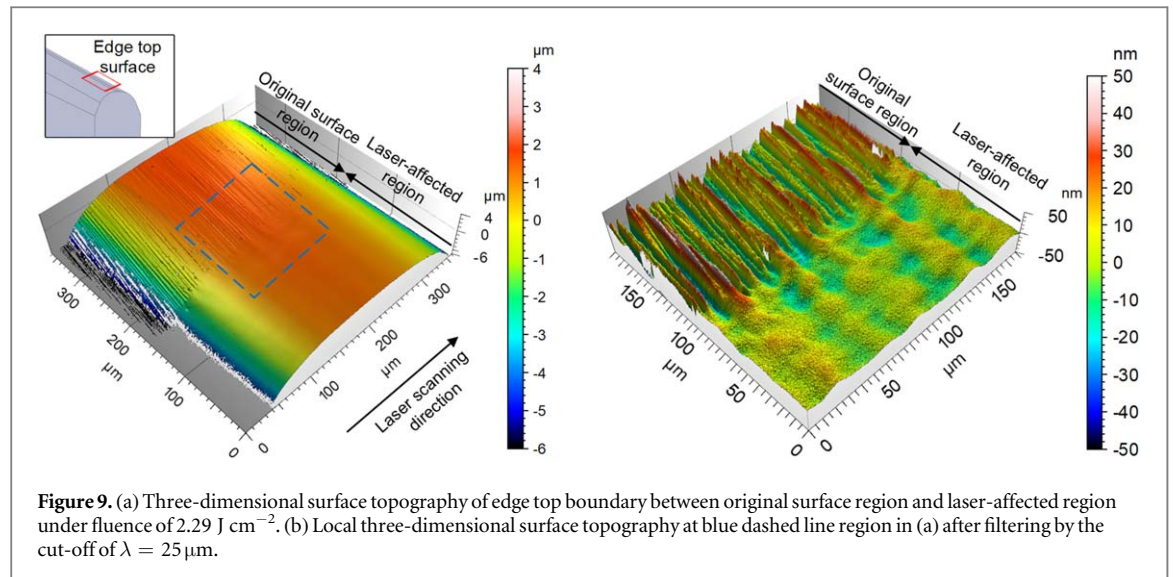
waviness still remained. This is because the melted silicon layer was extremely thin and the surface tension effect was limited to the top surface layer only. In addition, there were some voids on the surface after laser irradiation, indicating that the grinding-induced cracks remained open due to the insufficient melting of silicon. As laser fluence increased to 1.94 J cm<sup>-2</sup>, the waviness height decreased (figure 7(c)). This was because the thickness of melted silicon layer became larger, and accordingly the surface tension effect was enhanced. When the laser fluence increased to 2.29 J cm<sup>-2</sup>, the surface became flat and no voids were seen (figure 7(d)). Due to that the thickness of the melted layer was bigger than that of the grinding-induced cracks, surface tension effect was dominant over the entire surface. Thus, the initially rough surface became distinctly smoother. However, when the laser fluence reached 2.64 J cm<sup>-2</sup>, parallel grooves were observed on the surface, which were produced by the laser scan (figure 7(e)). Under this condition, laser ablation occurred, causing material removal from the surface [15, 16].

Figure 8 compares the surface roughness of the original surface, laser-affected surfaces, and CMP surface as a reference. Surface roughness decreased as laser fluence increased. Surface roughness was improved from 10.2 nmSa to 3.9 nmSa by laser irradiation. However, an inverse trend is observed at a laser fluence of 2.64 J cm<sup>-2</sup> due to the occurrence of grooves. The surface roughness of the laser-affected region is higher than that of the CMP wafer.

Figure 9(a) shows the three-dimensional surface topography of a wafer edge top surface near the boundary between the original ground region and the laser-affected region under laser fluence of 2.29 J cm<sup>-2</sup>. Grinding marks can be clearly observed on the ground surface. However, no grinding mark was found on the laser-affected region. Figure 9(b) is the local three-dimensional surface topography of the area within the blue dashed line region in figure 9(a). To avoid the waviness effect, the Gaussian filter was used by a cut-off of  $\lambda = 25 \mu\text{m}$ . It can be seen that after laser irradiation, a few sharp ridges of grinding marks were merged into broader smooth ridges.

### 4.2. Crystal structure evaluation of wafer edge top

Figure 10 shows Raman spectra of the original surfaces, the laser-affected surface under laser fluence of 2.29 J cm<sup>-2</sup>, and CMP surface as a reference. The Si-I (cubic diamond structure) peak (521 cm<sup>-1</sup>) was observed in each spectrum [17]. The peak intensity of the original surface at 521 cm<sup>-1</sup> was lower than that of the CMP surface. In contrast, the laser-affected surface shows similar peak intensity as the CMP surface. The Si-XII (rhombohedral structure, r8) peak (356 cm<sup>-1</sup>) was observed in the spectra of the original surface 1 [18]. However, there was no Si-XII peak in the original surface 2, the laser-affected surface and the CMP



**Figure 9.** (a) Three-dimensional surface topography of edge top boundary between original surface region and laser-affected region under fluence of  $2.29 \text{ J cm}^{-2}$ . (b) Local three-dimensional surface topography at blue dashed line region in (a) after filtering by the cut-off of  $\lambda = 25 \mu\text{m}$ .

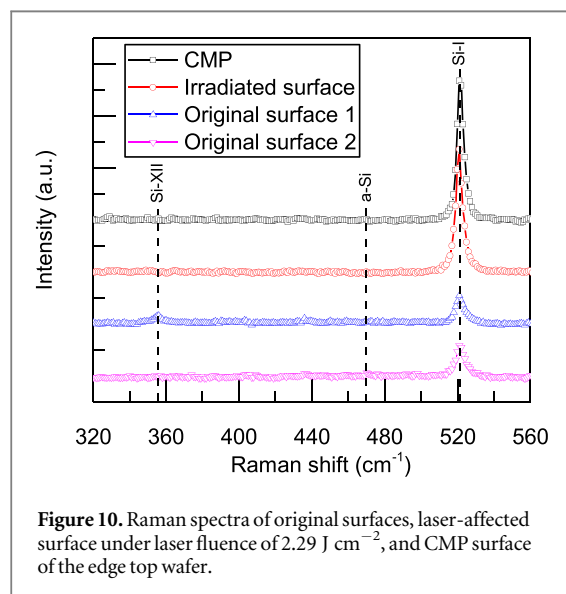


**Figure 10.** Raman spectra of original surfaces, laser-affected surface under laser fluence of  $2.29 \text{ J cm}^{-2}$ , and CMP surface of the edge top wafer.

surface. As shown in the spectra of the original surface 1 and 2, a part of the original surface has the Si-XII peak. Normally, amorphous silicon (a-Si) shows a broad peak at  $470 \text{ cm}^{-1}$  in a Raman spectrum [17]. However, in this study, the a-Si peak was too small to recognize in the Raman spectrum of the original surface in figure 10. Mapping measurement was further performed to evaluate the surface crystallinity for more details.

Figure 11(a) shows the surface micrograph of the edge top surface at the boundary between the original region and laser-affected region, where Raman mapping measurement points are indicated. Figure 11(b) shows the Raman mapping result at the Si-XII peak ( $356 \text{ cm}^{-1}$ ). The Si-XII phase existed in the original surface. However, the peak intensity of Si-XII in the laser-affected region was remarkably lower. Figure 11(c) shows the Raman mapping result at the

a-Si peak ( $470 \text{ cm}^{-1}$ ). The a-Si phase existed in the original surface. In contrast, the peak intensity of a-Si in the laser-affected region was obviously lower. From these results, it is clear that the grinding process has caused phase transformation of silicon from Si-I to Si-XII and a-Si simultaneously. After laser recovery, however, both Si-XII and a-Si were transformed back to Si-I.

As known in nanoindentation test of Si, when the unloading rate is very fast, or the indentation load is small, Si-I phase immediately transforms into amorphous phase through Si-II (metallic  $\beta$ -tin structure) phase [17, 18]. On the other hand, if the unloading rate is slow, Si-I phase transforms into Si-XII and Si-III (body-centered cubic structure) phases [17, 18]. From the results in figures 11(b), and (c), it is possible that the edge grinding process has induced not only a-Si phase, but also Si-XII phase.

Figure 11(d) shows the Raman mapping result at the Si-I peak ( $521 \text{ cm}^{-1}$ ). The intensity of Si-I in the laser-affected region was significantly higher than that in the original surface. From these results, it can be concluded that grinding-induced Si-XII and a-Si, as well as other possible phases, were completely changed into Si-I phase by laser irradiation.

### 4.3. Surface topography of wafer beveled edge

In order to compare the effect of laser fluence, figure 12 shows the local three-dimensional surface topography of the beveled edge of the original surface (figure 12(a)) and surface after laser irradiation with different fluences (figures 12(b) and (c)) after filtering by the cut-off of  $\lambda = 25 \mu\text{m}$ . There were no significant changes between the original beveled edge surface (figure 12(a)) and laser-affected surface with  $0.61 \text{ J cm}^{-2}$  (figure 12(b)). When laser fluence increased to  $1.58 \text{ J cm}^{-2}$ , it can be seen that sharp ridges of grinding marks were smoothed (figure 12(c)). The surface roughness of the beveled edge surface in

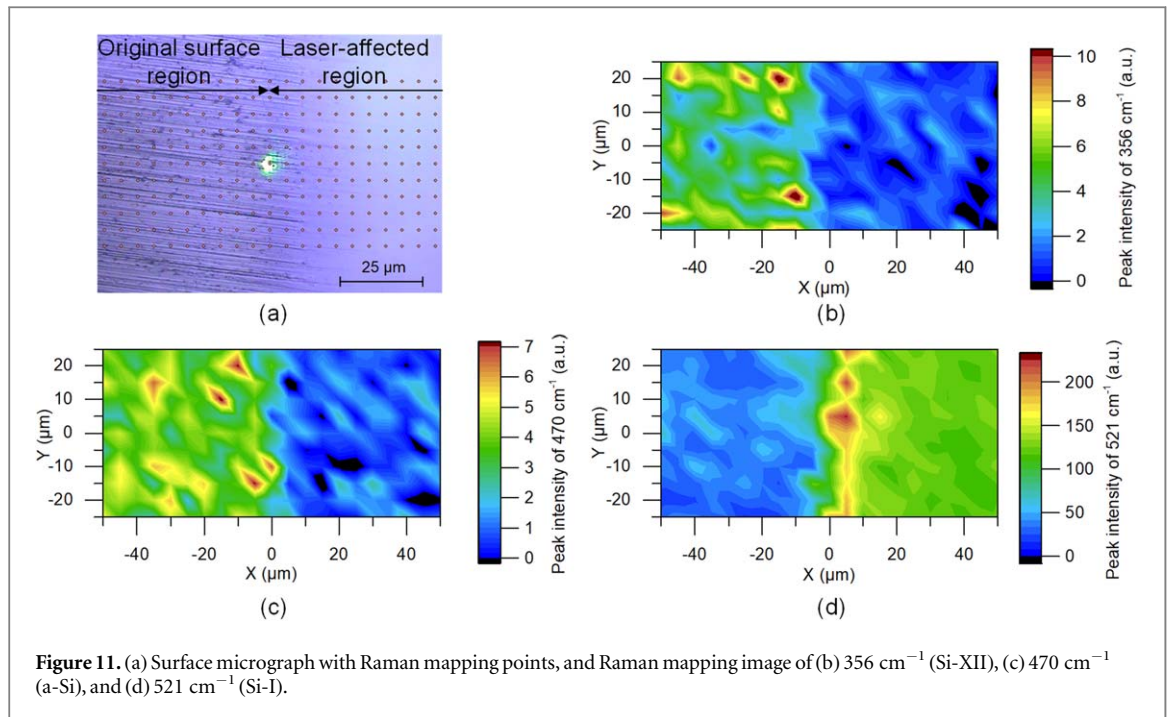


**Figure 11.** (a) Surface micrograph with Raman mapping points, and Raman mapping image of (b)  $356\text{ cm}^{-1}$  (Si-XII), (c)  $470\text{ cm}^{-1}$  (a-Si), and (d)  $521\text{ cm}^{-1}$  (Si-I).

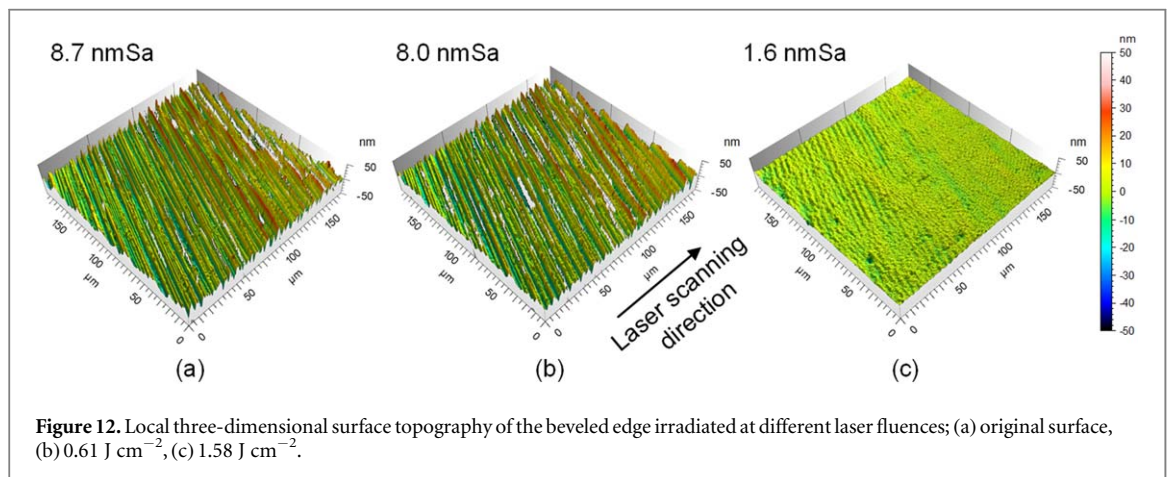


**Figure 12.** Local three-dimensional surface topography of the beveled edge irradiated at different laser fluences; (a) original surface, (b)  $0.61\text{ J cm}^{-2}$ , (c)  $1.58\text{ J cm}^{-2}$ .

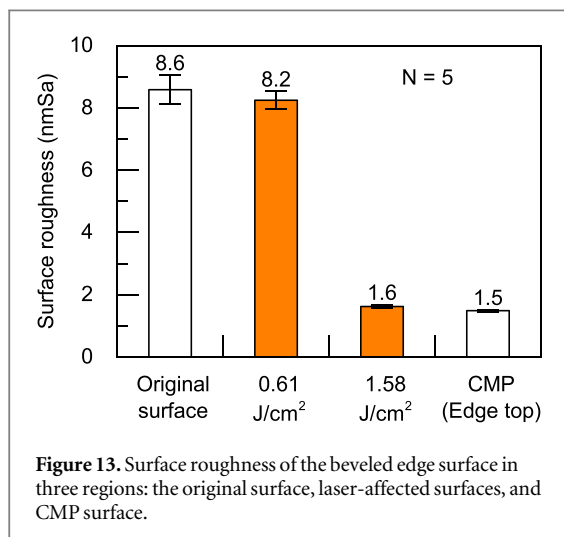


**Figure 13.** Surface roughness of the beveled edge surface in three regions: the original surface, laser-affected surfaces, and CMP surface.

several regions: original surface, laser-affected surfaces, and CMP surface is presented in figure 13. Surface roughness was improved from 8.6 nmSa to 1.6 nmSa by laser irradiation. The surface roughness of laser-affected region with  $1.58\text{ J cm}^{-2}$  achieved almost same quality of the CMP wafer.

In comparison with surface roughness of the edge top which was 3.9 nmSa, the surface roughness of the beveled edge which was 1.6 nmSa was low as shown in figures 8 and 13. There might be two reasons for the difference in the improved surface roughness of these two types of surface. First, the original surface roughness of beveled edge was smaller than that of edge top. If the surface roughness of the original surface is smaller, the melting surface is smoothed by laser irradiation. Second, the volume of melting layer on the

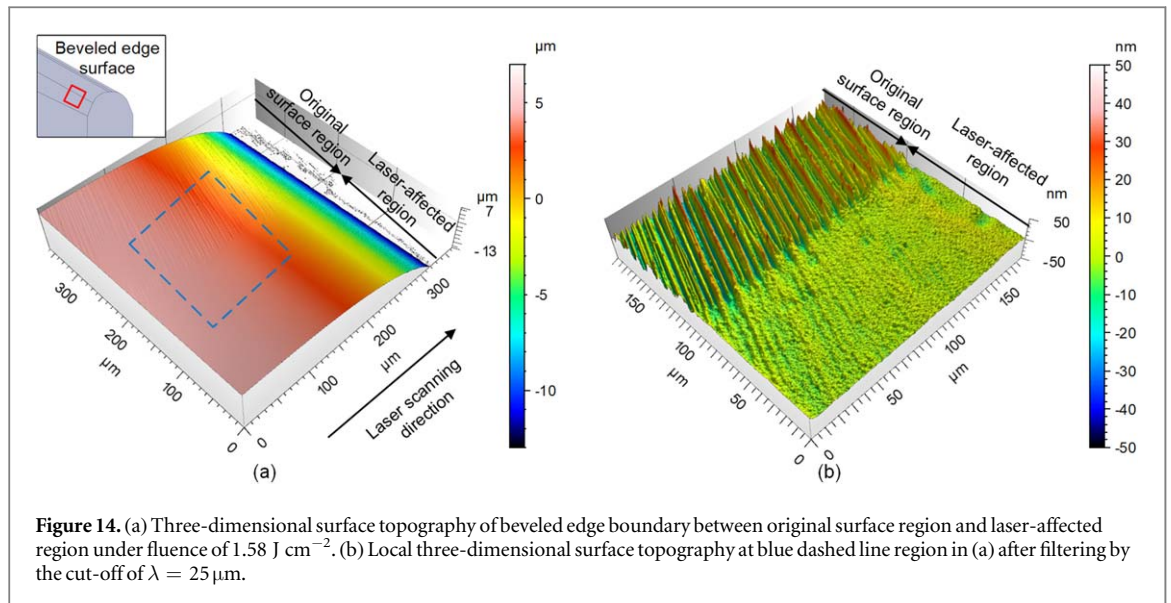


**Figure 14.** (a) Three-dimensional surface topography of beveled edge boundary between original surface region and laser-affected region under fluence of  $1.58 \text{ J cm}^{-2}$ . (b) Local three-dimensional surface topography at blue dashed line region in (a) after filtering by the cut-off of  $\lambda = 25 \mu\text{m}$ .

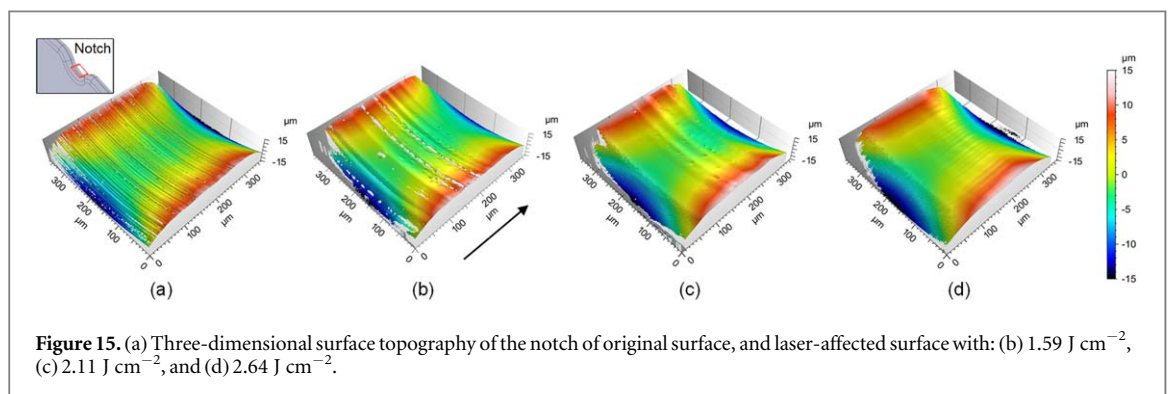


**Figure 15.** (a) Three-dimensional surface topography of the notch of original surface, and laser-affected surface with: (b)  $1.59 \text{ J cm}^{-2}$ , (c)  $2.11 \text{ J cm}^{-2}$ , and (d)  $2.64 \text{ J cm}^{-2}$ .

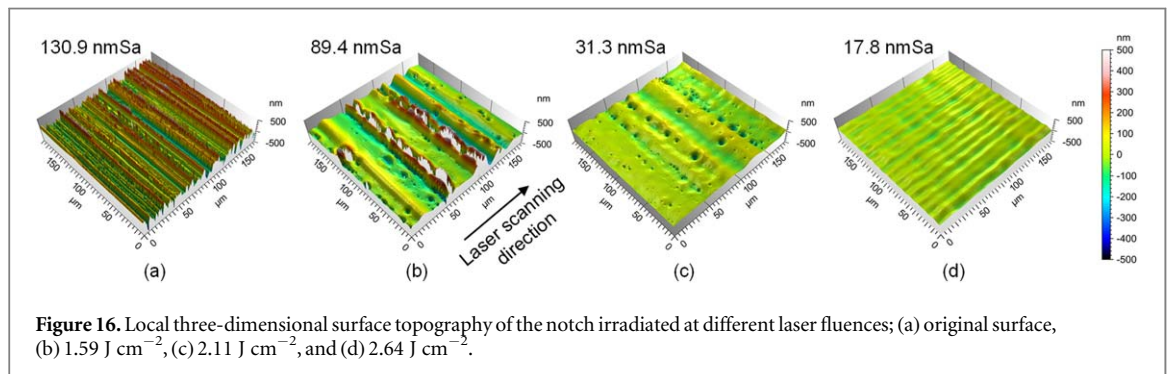


**Figure 16.** Local three-dimensional surface topography of the notch irradiated at different laser fluences; (a) original surface, (b)  $1.59 \text{ J cm}^{-2}$ , (c)  $2.11 \text{ J cm}^{-2}$ , and (d)  $2.64 \text{ J cm}^{-2}$ .

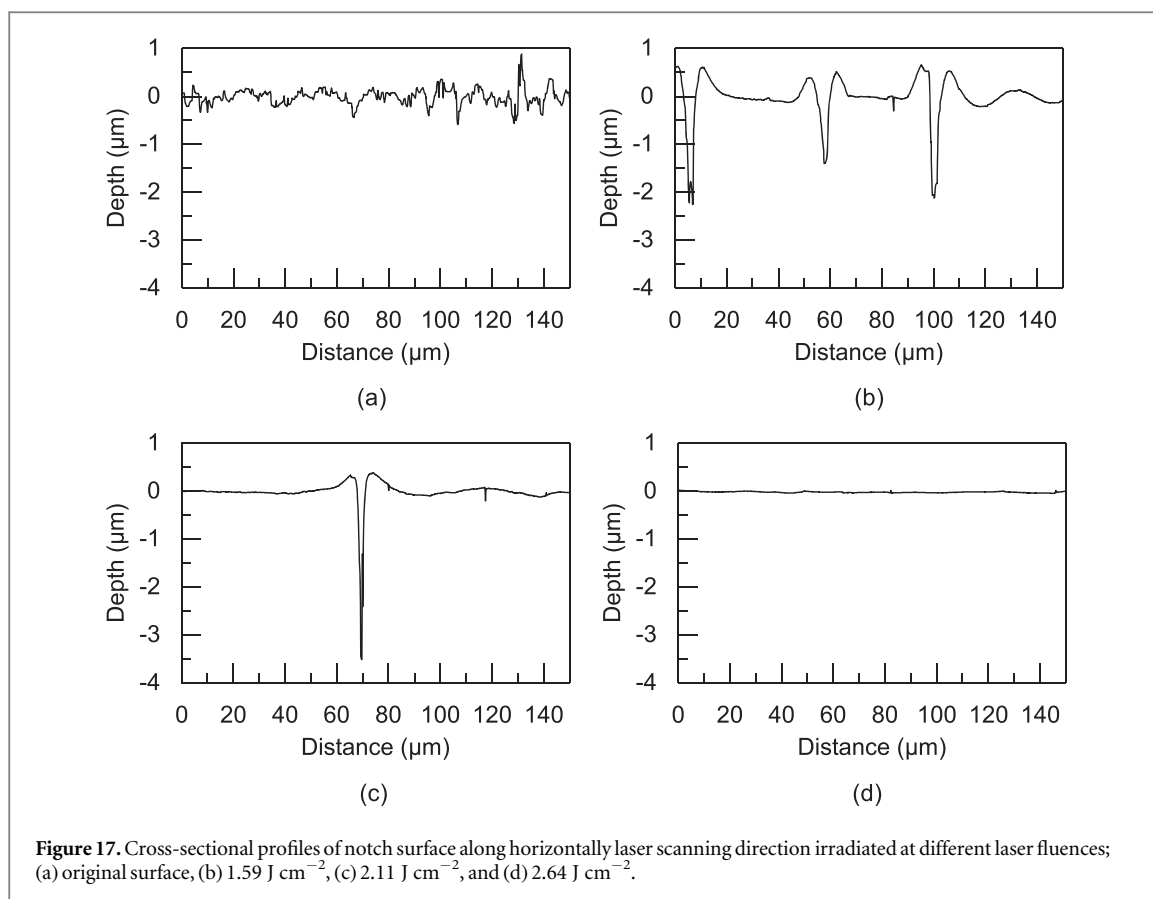
beveled edge was larger than that on the edge top due to the change of laser spot area. The volume of the melting layer affects the time of recrystallization. Enough time of recrystallization makes top surface smooth.

Figure 14(a) shows the three-dimensional surface topography of beveled edge boundary between the original surface and laser-affected region. There were grinding marks on the original surface while grinding marks were smoothed on laser-affected region. Figure 14(b) shows the local three-dimensional surface topography at blue dashed line region in

figure 14(a). To separate waviness effect, Gaussian filter was used by the cut-off of  $\lambda = 25 \mu\text{m}$ . After laser irradiation, sharp ridges of grinding mark became smooth.

#### 4.4. Laser recovery of wafer notch

Figure 15 shows the three-dimensional surface topography of a wafer notch before (figure 15(a)) and after laser irradiation (figures 15(b)–(d)). There were significant grinding marks on the original surface. Although the laser irradiation conditions used for the notch was the same as those for the edge top surface,



**Figure 17.** Cross-sectional profiles of notch surface along horizontally laser scanning direction irradiated at different laser fluences; (a) original surface, (b)  $1.59 \text{ J cm}^{-2}$ , (c)  $2.11 \text{ J cm}^{-2}$ , and (d)  $2.64 \text{ J cm}^{-2}$ .

deeper microcracks existed along the grinding marks on the notch surface, as shown in figure 15(b). When laser fluence increased as shown in figure 15(c), the number of microcracks decreased. When a further higher laser fluence  $2.64 \text{ J cm}^{-2}$  was used, there were no microcracks on the notch surface (figure 15(d)). Figure 16 is the local three-dimensional surface topography of the notch after filtering by a cut-off of  $\lambda = 25 \mu\text{m}$ . After laser irradiation, open cracks were observed in figure 16(b). When laser fluence increased (figure 16(b)), the number of microcracks were partially reduced (figure 16(c)). However, several microcracks still remained on the notch surface. When a further higher laser fluence of  $2.64 \text{ J cm}^{-2}$  was used, microcracks completely disappeared (figure 16(d)). Under this condition, there was a waviness perpendicular to the scanning direction. The waviness might have been caused by convection of liquid silicon or laser-induced plasma pressure during the laser irradiation process.

In order to investigate the depth of microcracks, cross-sectional profiles were measured along the laser scanning direction in figure 16. Figure 17 shows cross-sectional profiles of the notch surface after filtering by a cut-off of  $\lambda = 25 \mu\text{m}$ . Microcracks with depth over  $1 \mu\text{m}$  was not observed in figure 17(a). In figures 17(b), and (c), however, open microcracks with depth over  $1 \mu\text{m}$  appeared. In contrast, at a high fluence of  $2.64 \text{ J cm}^{-2}$ , the notch surface was smooth, and there were no microcracks at all.

Based on the analysis of the open microcracks, the mechanism of laser recovery of microcracks with different laser fluences is shown in figure 18. Grinding-induced microcracks are usually formed under the amorphous layer [2]. Thus, it is difficult to measure the internal microcracks from the surface. When laser fluence is not high enough to recover the microcracks, which means the recrystallized depth is smaller than the depth of the microcracks (figure 18(a)), the microcracks will open after laser irradiation (figure 18(b)). By increasing laser fluence (figure 18(c)), most of the microcracks are recovered by laser irradiation. However, the microcrack which is deeper than the recrystallized depth will remain on the surface as an open crack (figure 18(d)). By irradiating a laser with higher fluence which can melt and recrystallize deeper material than the microcracks (figure 18(e)), the microcracks will be completely recovered (figure 18(f)).

Figure 19 is a comparison of surface roughness of a notch surface before and after laser irradiation. The surface roughness of a CMP surface was also shown as a reference. Surface roughness was significantly improved from  $131.3 \text{ nmSa}$  to  $19.6 \text{ nmSa}$  by laser irradiation, although the surface roughness of laser affected region is still higher than that of the CMP surface.

#### 4.5. Effect of laser irradiation on material hardness

Figure 20 shows the change of indentation depth of a ground wafer after laser irradiation and a CMP wafer as the reference with various indentation loads.

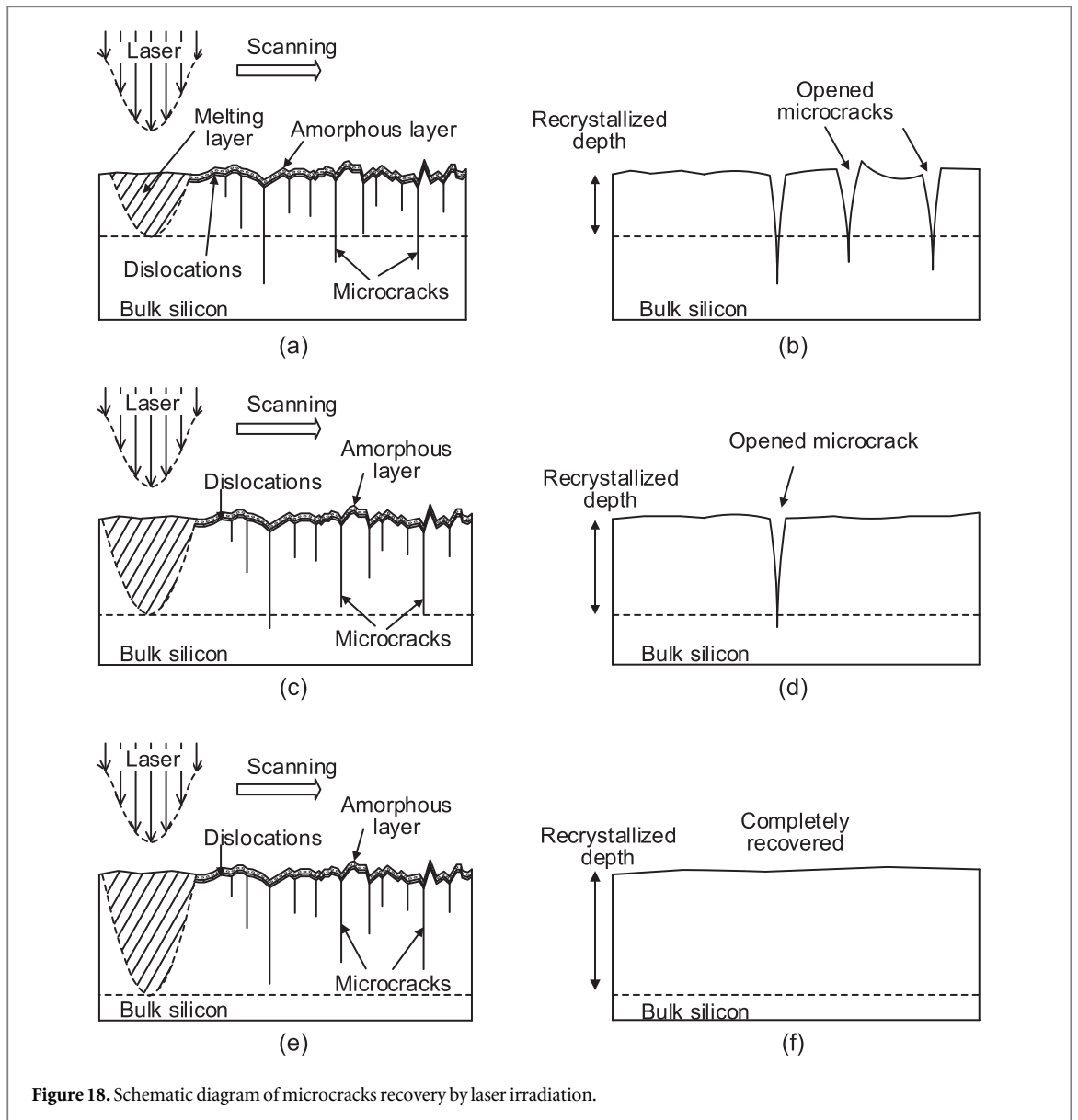


Figure 18. Schematic diagram of microcracks recovery by laser irradiation.

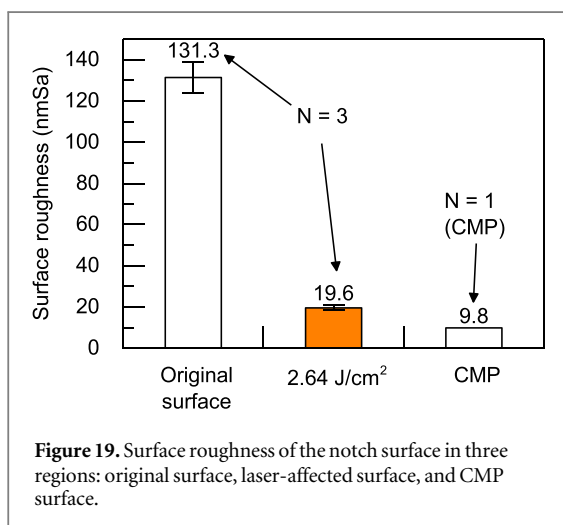


Figure 19. Surface roughness of the notch surface in three regions: original surface, laser-affected surface, and CMP surface.

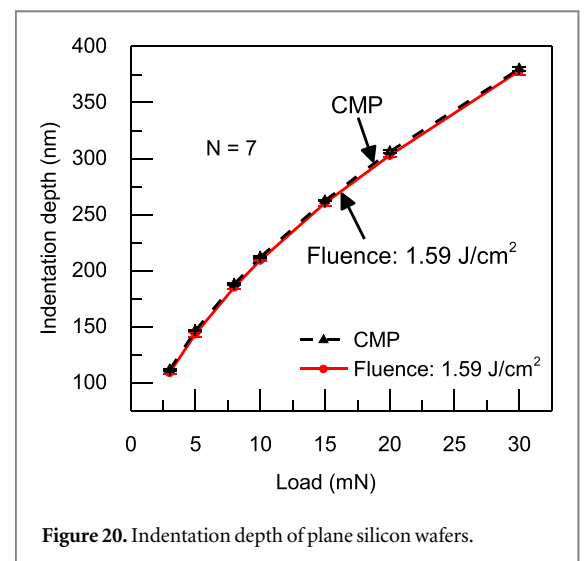


Figure 20. Indentation depth of plane silicon wafers.

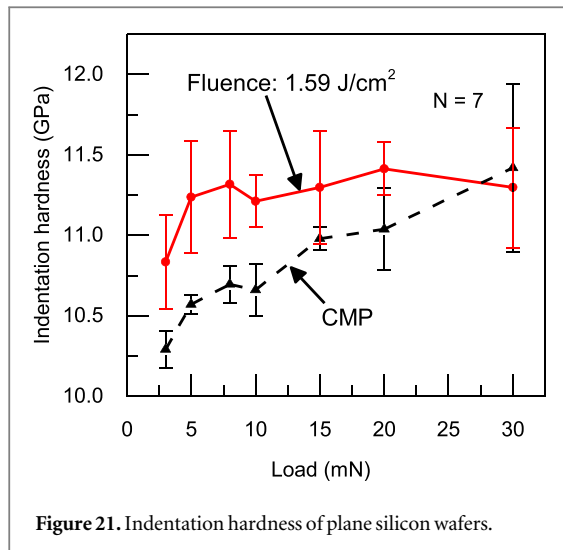


Figure 21. Indentation hardness of plane silicon wafers.

Indentation depth ranges from 110 nm to 380 nm with the increase of indentation load. Figure 21 shows the calculated indentation hardness of the two types of wafers. Indentation hardness shows a difference between the laser-affected wafer and the CMP wafer in the small load range (3–10 mN). In case of the high load range (>15 mN), however, the difference of indentation hardness is insignificant.

Indentation hardness of a thin film is affected by the substrate [19]. In this study, it is assumed that the laser recovered layer is as with a thin film on the bulk silicon substrate. As known from the previous research [12], the laser recrystallized depth was 653 nm at an energy density of  $1.59 \text{ J cm}^{-2}$ . The difference of hardness is significant when indentation depth becomes smaller. At a higher load, the difference becomes insignificant due to the increasing effect of the bulk region.

The melting and recrystallizing process by laser irradiation lead to migration of dopant in the irradiated region. The segregation coefficient  $k_p$ , which describes the relation between the concentration of impurity atoms in the growing crystal and that of the melt, is defined by:

$$k_p = \frac{C_l}{C_s} \quad (6)$$

where  $C_s$  is dopant concentration in the solid phase silicon, and  $C_l$  is that in the liquid phase silicon. Generally, the segregation coefficient  $k_p$  in equilibrium condition for boron in silicon is 0.8 [20]. In case of rapid solidification after nanosecond pulsed laser irradiation, however, the segregation coefficient  $k_p$  becomes 1.25 [20]. In a supercooling state due to rapid solidification, liquid-liquid phase transition (LLPT) occurs from the metallic bonding composing high-density liquid to the covalent bonding making low-density liquid [21]. The low-density liquid with the covalent bonding makes boron atoms difficult to move from the interface to the surface. Thus, the dopant concentration becomes minimum at the top surface

layer [12, 22, 23]. It is known that the indentation hardness of lightly doped silicon is higher than that of heavily doped silicon wafer [24], thus it is presumable that the difference of indentation hardness was caused by the decrease of dopant concentration at top surface layer due to laser irradiation.

The increase of surface hardness of wafer edge and notch is beneficial because it will enhance the mechanical strength of a wafer, thus the resistance to mechanical wear and impacts will be improved. This will help to prevent both wafer breakage and particle contamination during wafer handling.

## 5. Conclusions

Nanosecond pulsed laser irradiation was performed for the edge and notch of a boron-doped single-crystal silicon wafer after diamond grinding. The main findings include:

1. The surface roughness of wafer edge top was improved from 10.2 nmSa to 3.9 nmSa by laser irradiation. In addition, grinding-induced Si-XII and a-Si phases were completely recrystallized into Si-I phase by using laser irradiation.
2. Laser was irradiated on the beveled edge surface at different angles of incident. The surface roughness of beveled edge was improved to 1.6 nmSa by irradiating with laser fluence of  $1.58 \text{ J cm}^{-2}$ .
3. By laser irradiation with sufficiently high laser fluence, the grinding-induced internal microcracks in the wafer notch were completely eliminated. The surface roughness of the notch was improved from 131.3 nmSa to 19.6 nmSa by laser irradiation.
4. The indentation hardness of laser irradiated silicon wafer was higher than that of a CMP wafer. The difference of hardness was caused by the decrease in dopant concentration at the top surface layer due to laser irradiation. Surface hardening improves the mechanical strength of a wafer.

The findings from this study will contribute to the manufacturing of high-quality silicon wafers. Future work includes optimizing laser fluence and beam shape for rapid processing of an entire wafer having complicated shaped surfaces.

## Acknowledgment

This work has been partially supported by Keio University Doctorate Student Grant-in-Aid Program.

## ORCID iDs

Jiawang Yan  <https://orcid.org/0000-0002-5155-3604>

## References

- [1] Yan J, Asami T, Harada H and Kuriyagawa T 2009 Fundamental investigation of subsurface damage in single crystalline silicon caused by diamond machining *Precis. Eng.* **33** 378–86
- [2] Kovalchenko A M and Milman Y V 2014 On the cracks self-healing mechanism at ductile mode cutting of silicon *Tribol. Int.* **80** 166–71
- [3] Li H N, Yu T B, Zhu L D and Wang W S 2017 Analytical modeling of grinding-induced subsurface damage in monocrystalline silicon *Mater. Des.* **130** 250–62
- [4] Chen P Y, Tsai M H, Yeh W K, Jing M H and Chang Y 2010 Relationship between wafer edge design and its ultimate mechanical strength *Microelectron. Eng.* **87** 2065–70
- [5] Chen P Y, Tsai M H, Yeh W K, Jing M H and Chang Y 2010 Relationship between wafer fracture reduction and controlling during the edge manufacturing process *Microelectron. Eng.* **87** 1809–15
- [6] Chen P Y, Tsai M H, Yeh W K, Jing M H and Chang Y 2009 Investigation of the relationship between whole-wafer strength and control of its edge engineering *Jpn. J. Appl. Phys.* **48**
- [7] Robert D and Yoshio N 2007 *Handbook of Semiconductor Manufacturing Technology* (Boca Raton: Taylor & Francis Group) 1720
- [8] Pei Z J, Fisher G R and Liu J 2008 Grinding of silicon wafers: a review from historical perspectives *Int. J. Mach. Tools Manuf.* **48** 1297–307
- [9] Yan J, Asami T and Kuriyagawa T 2007 Response of machining-damaged single-crystalline silicon wafers to nanosecond pulsed laser irradiation *Semicond. Sci. Technol.* **22** 392–5
- [10] Yan J, Sakai S, Isogai H and Izunome K 2009 Recovery of microstructure and surface topography of grinding-damaged silicon wafers by nanosecond-pulsed laser irradiation *Semicond. Sci. Technol.* **24** 6
- [11] Yan J and Kobayashi F 2013 Laser recovery of machining damage under curved silicon surface *CIRP Ann. - Manuf. Technol.* **62** 199–202
- [12] Niitsu K, Tayama Y, Kato T, Maehara H and Yan J 2018 Characterization of recrystallized depth and dopant distribution in laser recovery of grinding damage in single-crystal silicon *Mater. Sci. Semicond. Process.* **82** 54–61
- [13] Steen W M and Mazumder J 2010 *Laser Material Processing* 4th (London: Springer-Verlag) 558
- [14] Wang H, Liu X and Zhang Z M 2013 Absorption coefficients of crystalline silicon at wavelengths from 500 nm to 1000 nm *Int. J. Thermophys.* **34** 213–25
- [15] Bennett T D, Krajnovich D J, Grigoropoulos C P, Baumgart P and Tam A C 1997 Marangoni mechanism in pulsed laser texturing of magnetic disk substrates *J. Heat Transfer* **119** 589
- [16] Tam A C, Pour I K, Nguyen T, Krajnovich D and Baumgart P 1996 Experimental and theoretical studies of bump formation during laser texturing of Ni-P disk substrates *IEEE Trans. Magn.* **32** 3771–3
- [17] Gogotsi Y, Baek C and Kirscht F 1999 Raman microspectroscopy study of processing-induced phase transformations and residual stress in silicon *Semicond. Sci. Technol.* **14** 936–44
- [18] Huang H and Yan J 2016 Volumetric and timescale analysis of phase transformation in single-crystal silicon during nanoindentation *Appl. Phys. A* **122** 607
- [19] Saha R and Nix W D 2002 Effects of the substrate on the determination of thin mechanical properties by nanoindentation *Acta Mater.* **50** 23–8
- [20] Lill P C, Dahlinger M and Köhler J R 2017 Boron partitioning coefficient above unity in laser crystallized silicon *Materials (Basel)*. **10** 189
- [21] Okada J T et al 2012 Persistence of covalent bonding in liquid silicon probed by inelastic x-ray scattering *Phys. Rev. Lett.* **108** 067402
- [22] Lombardo S F et al 2017 Laser annealing in Si and Ge: anomalous physical aspects and modeling approaches *Mater. Sci. Semicond. Process.* **62** 80–91
- [23] Fiscaro G, Huet K, Negru R, Hackenberg M, Pichler P, Taleb N and La Magna A 2013 Anomalous impurity segregation and local bonding fluctuation in l-Si *Phys. Rev. Lett.* **110** 117801
- [24] Bhushan B and Li X 1997 Micromechanical and tribological characterization of doped single-crystal silicon and polysilicon films for microelectromechanical systems devices *J. Mater. Res.* **12** 54–63